

## **Distribution Measurement and Mechanism Research on Deformation due to Losing Water of Overburden Layer**

Chunde Piao, Jun Yuan, Dangliang Wang, Pengtao Li

*School of Resources and Geosciences, China University of Mining and Technology, Xuzhou, Jiangsu 221116, China, Email: piaochunde@126.com*

**Abstract** Based on FBG fiber Bragg grating technology and BOTDA distributed optical fiber sensing technology, this study used fine sand to simulate overburden layer in vertical shaft model equipment. The placing technique and test method for optical fiber sensors in the overburden layer were studied, combined with MODFLOW software to simulate the change of the water head value when the overburden layer was losing water, and obtained the deformation features of overburden layer. The results showed that at the beginning of water loss, the vertical deformation increased due to larger hydraulic pressure drop, while the deformation decreased gradually and tended to be stable with the hydraulic pressure drop reducing. The circumferential deformation was closely related to the distance between the drainage holes, variations of water head value and the method of drainage. The monitoring result based on optical fiber sensing technology was consistent to the characteristics of water loss in overburden layer simulated by MODFLOW software, which showed that the optical fiber sensing technology applied to monitor shaft overburden layer was feasible.

**Keywords** overburden layer, BOTDA, fiber bragg grating, distributed monitoring technology, water loss

### **Introduction**

A series of problems have cropped up in coal mining, the shaft lining rupture and local buckling deformation is always a major problem. Since the mine disaster caused by rupture of shaft lining, through a large number of theoretical studies and testing data, it is proved that the vertical additional force which results from consolidation settlement due to drainage in thick overburden is the major factor which could lead to rupture of shaft lining. At present, to monitor the shaft deformation, most researches analyze stability of the shaft lining structure by geometric metrology or the sensors installed the outer part of shaft lining<sup>4</sup>, but monitoring methods of overburden settlement are studied less before. If overburden could be effectively monitored and the hydrophobic settlement deformation characteristics could be timely recognized during operation of shaft lining, it will be possible to take effective measures to avoid the occurrence of fatal accidents.

As one of the most promising technology in fiber optic sensor, distributed optical fiber sensing technology has many advantages, such as distributed monitor, long distance, anti-electromagnetic interference, corrosion resistance, great durability, small size, light weight, etc. This technology has been widely used in engineering field including slope, pile foundation, tunnel, etc. Facing the current situation of serious rupture of shaft lining, this paper, based on FBG fiber grating technology and BOTDA optical fiber sensing technology, uses the test device of shaft model, studies the placing technique for optical fiber sensors in the overburden layer, establishes the monitoring method based on optical fiber sensing technology, and analyzes hydrophobic settlement deformation characteristics, thus providing theoretical support and technical indemnification for exploitation of coal resources.

### **Optical fiber sensor monitoring technique**

#### ***Fiber bragg grating technology***

In 1978, Hill K.O. et al. at Communications Research Centre in Ottawa, Canada first found photosensitivity in a Germanium-doped silica fiber, and made the first one optical fiber grating sensor by using standing wave method. With research all over the world increasing,

Fiber Bragg Grating Sensor has become most widely used Optical Fiber Sensor in health monitoring. The basic principle of Fiber Bragg Grating Sensor is that when the broadband incident light enters the fiber, the light which meets wave length conditions of Bragg grating will be reflected to become reflection light, and the rest of the light will become transmitted light. External temperature and strain changes will cause wavelength shift of reflection light, so by detecting the change of center wavelength, the change of measured signal can be obtained. The relationship between the strain and the center wavelength of fiber grating plus temperature is as following.

$$\frac{\Delta\lambda_B}{\lambda_B} = c_\varepsilon\Delta\varepsilon + c_T\Delta T \quad (1)$$

In the above formula,  $\lambda_B$  and  $\Delta\lambda_B$  are respectively the initial central wavelength of reflection light and the drift amount of central wavelength.  $\Delta\varepsilon$  and  $\Delta T$  are the variable quantity of strain and temperature.  $c_\varepsilon$  and  $c_T$  are strain coefficient and temperature coefficient of fiber Bragg grating. At present, temperature accuracy of fiber Bragg grating is  $0.1^\circ\text{C}$  and strain accuracy is  $1\ \mu\varepsilon$ .

### ***Brillouin optical time-domain analysis***

Brillouin Optical Time-Domain Analysis (BOTDA) was first proposed by Horiguchi T. et al. in 1989, then it was applied to fiber lossless measurement in fiber communication field. Its spatial resolution was 100 m and strain accuracy was  $100\ \mu\varepsilon$ .

Kishida K. et al. introduced the Pre-pumped Pulse method based on the theory model of leakage light pumped pulse. The Neubrex company developed type NBX-6000Pulse-PrePumpBrillouin Optical Time-Domain Analyzer (PPP-BOTDA). The measuring principle of PPP-BOTDA is that by changing the structure of pumping laser pulse, both ends of fiber are respectively injected with step Index pump pulse light and continuous light, and pre pump pulse stimulates acoustic wave before pump pulse arrives detection zone, thus pre pump pulse, pump pulse, probe laser and stimulated acoustic wave interact with each other in the fiber, creating stimulated Brillouin scattering. Through the continuous frequency adjustment of the exploring laser light source, the continuous light power output is detected from the other end of fiber, which determines the frequency difference when fiber's Brillouin gain maximum in every small area, and this frequency difference is equal to fiber's Brillouin frequency shift in each part of area. Thus, according to the linear relation of Brillouin frequency shift and strain temperature, the change of strain and temperature can be determined of the various points along the fiber and it is as shown in expression (2).

$$v_B(\varepsilon, T) = v_B(0) + \frac{dv_B(\varepsilon)}{d\varepsilon} \cdot \varepsilon + \frac{dv_B(T)}{dT} \cdot (T - T_0) \quad (2)$$

In the above formula,  $v_B(\varepsilon, T)$  is the drift amount of fiber Brillouin frequency with the change of strain and temperature, while  $v_B(0)$  is the drift amount of fiber Brillouin frequency without the change of strain and temperature.  $\varepsilon$  is the axial dependent variable of sensing optical fiber.  $(T - T_0)$  is the variable quantity of external temperature.  $dv_B(\varepsilon)/d\varepsilon$  and  $dv_B(T)/dT$  are respectively influence coefficient of strain and temperature.

At present, the minimum spatial resolution of 10cm can be reached and strain accuracy is  $25\ \mu\varepsilon$  in measurement range of 1km when this measurement technique is applied.

### **Model test on deformation in overburden layer**

### Test scheme

Through simulating overburden layer with fine sand, this experiment used the self-made vertical shaft model equipment to study the settlement and deformation, which resulted from the drainage in overburden layer. The diameter of the model equipment was 1400 mm and the height of the model equipment was 870 mm. The diameter of the shaft lining was 220 mm. There were two drainage holes at the bottom of the model equipment and three central drainage holes were 410 mm above from the bottom, with the diameter of all the drainage holes being 20 mm. The height of fine sand was 730 mm. During the test medium, the nonuniform coefficient( $C_u$ ) of fine sand was 2.56, and the curvature coefficient ( $C_c$ ) was 1.03. The permeability coefficient was 9 m/d; the water storage capacity was 0.1; the effective porosity was 0.1. The specific size of the model equipment was shown in fig. 1.

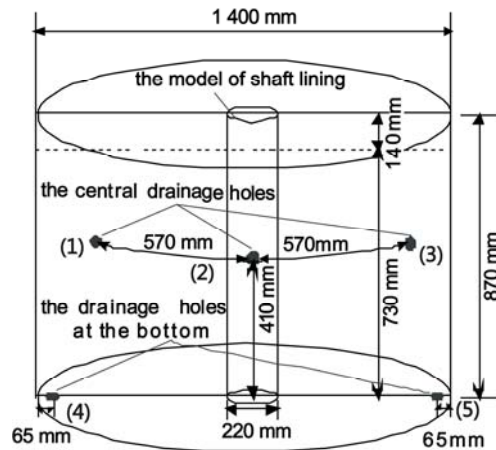
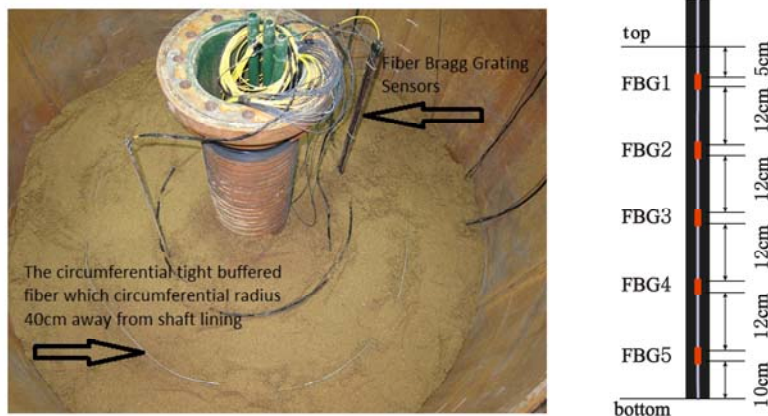


Fig.1 The size of shaft lining model equipment

To measure the vertical settlement and circumferential deformation caused by the overburden losing water, we laid FBG optical fiber grating sensors and tight buffered optical fibers on the vertical and circumferential directions. Based on the layout scheme, 200 mm above from the bottom of the model equipment, we put every 100 mm distance, 5 circumferential tight buffered fibers, whose circumferential radius is 400 mm away from shaft lining. The iron plate with width of about 20 mm and length of about 750 mm was installed about 200 mm away from the shaft lining between the shaft lining and the central drainage hole 2. Five sensors FBG were pasted on the iron plate which length was 10 mm. The layout method of optical fiber sensors and the size of FBG optical fiber grating sensors were shown in fig. 2. The sensors FBG2 and FBG3 failed during the test.

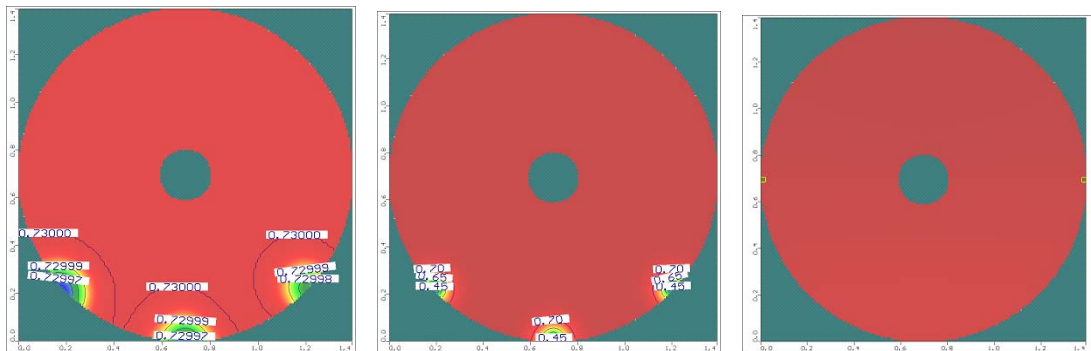
The bearing plate with thickness of 10 mm and diameter of 1360 mm was set on the top of fine sand layer in the experiment, whose weight was about 745 N. The jack and the weight were installed on the bearing plate to simulate earth pressure. The test was carried out in two steps. The first step was putting the weights of 1000 N, 3000 N and 5000 N on the bearing plate to study the vertical and circumferential deformation of fine sand layer in the function of the upper pressure before water injection test. The second step was injecting water to the top of fine sand layer, and then opening both central drainage holes and bottom drainage holes simultaneously, in order to study consolidation settlement and circumferential deformation of fine sand layer caused by the drainage.



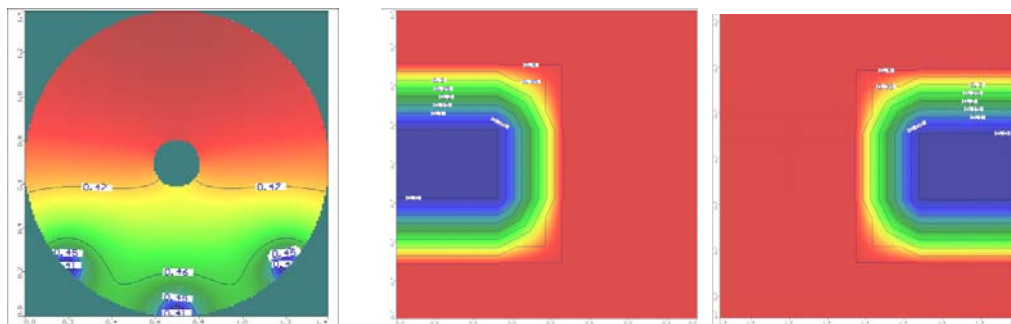
(a) The layout method of optical fiber sensors (b) The size of FBG optical fiber grating sensors  
**Fig.2** The layout method of optical fiber sensors and the size of FBG optical fiber grating sensors

**Analysis on water loss of fine sand layer by MODFLOW software**

Based on the model of shaft lining, this study used the finite difference software Visual MODFLOW to construct the two-dimensional seepage model and got the change of head value when the fine sand layer lost water. The central drainage holes and the drainage holes at the bottom were opened at the same time. Fig. 3 was the variation distribution map of water head value when the fine sand layer began to lose water, and fig. 4 was the variation distribution map of water head value when the water level reached the central drainage holes.



(a) The plane on top of overburden layer (b) The plane 0.41m away from the bottom (c) The plane on bottom of overburden layer  
**Fig.3** The distribution map showing the variation of water head value of overburden layer at drainage time



(a) The plane 0.41m away from the bottom (b) The plane on bottom of overburden layer  
**Fig.4** The distribution map of the variation of water head value of overburden layer when the water level reached 0.41m

From fig. 3(a) and 3(c), at drainage time, the water head value on both top and bottom of overburden layer had relatively minor change. However, fig. 3(b) showed that, under the influence of central drainage holes, the water head value of plane 0.41 m away from the bottom changed greatly, yet its influence scope was only near the drainage holes. As shown in fig. 4(a), when the water level reached 0.41m, the water head value near the drainage holes decreased significantly, and the range of influence were between the central drainage holes and the head line whose value was 0.46, but the value at other position remained unaffected. Fig. 4(b) showed that, near the drainage holes at the bottom, the water head value of plane 0m would drop, but its influence scope was relatively small.

## Result analysis on deformation monitoring of overburden layer

### *Settlement and Compression Deformation of Overburden Layer Caused by Loading*

The deformation of fine sand layer which changed along with variation of time by using the sensors FBG1, FBG4 and FBG5 to monitor is shown in fig. 5, when applying the weights of 1000 N, 3000 N and 5000 N on the bearing plate.

Fig. 5 showed that the deformation of fine sand layer gradually increased with the load increasing under changeable load, while the deformation gradually reduced with the depth increasing. For the sensors FBG4 and FBG5 at the bottom of fine sand layer, the deformation curve was obviously stepped because the fine sand layer completed settlement and tend to be stable in a short time. For the sensor FBG1 installed on the top of fine sand layer, the deformation was small and temporary with lower loads. When loads increased, the soil pore was gradually filled with solid particles and the linear deformation intensified.

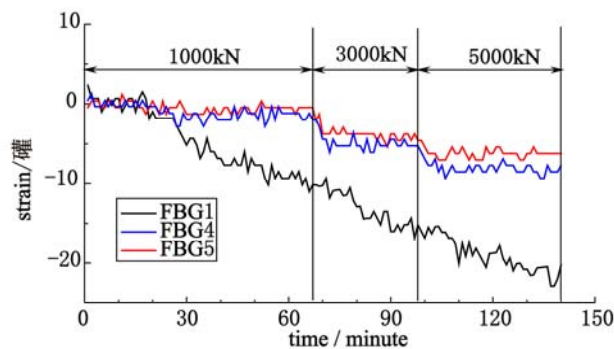


Fig.5 Dependent variable of fine sand layer along with variation of time under load

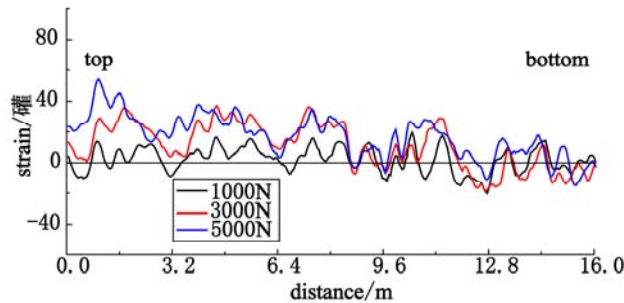
Using BOTDA distributed fiber sensing technology, we detected the annulus sensing fiber which was 40cm far away from the shaft lining, and got the value of the circumferential deformation of fine sand layer under changeable loads, as shown in fig. 6.

As shown in fig. 6, the circumferential deformation of fine sand layer increased with the load rising, and its value gradually dropped from the top to bottom; only soil was compressed under load, and the change of hoop strain at the same level was the same.

### *Settlement and compression deformation caused by water loss of the aquifer*

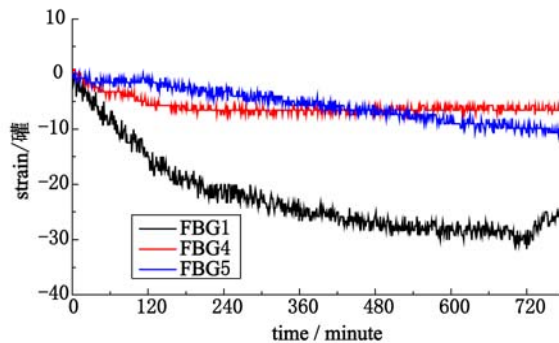
We analyzed the settlement character of the mine shaft, applying 5000 kN load to the laminate on the top of overburden layer, injecting water into the model equipment of shaft by the central drainage holes until the fine sand layer were submerged, then subsequently we opened central drainage holes and drainage holes at the bottom. Water level reached the central drainage holes when injecting water to the shaft about 80 minutes. The fine sand layer

continued to lose water with the drainage holes at the bottom with time going on. The settlement character of the fine sand layer when losing water was shown in fig. 7.



**Fig.6** Circumferential deformation of fine sand layer 40 cm away from the shaft lining under load

From fig. 7, during the fine sand layer losing water, the effective stress increased and the pore water pressure decreased. The fine sand was in transit from loose to dense state and gradually stabilized top-down. The deformation of the sensors depended on buried depth and water losing conditions. For the sensor FBG1 at the top of sand layer, the deformation increased with the initial increased water pressure drop. With the decrease of water pressure drop, the deformation became smaller gradually and tend to be stable. For the sensor FBG4, the fine sand deformation increased gradually with its water loss. As the sensor was located below drainage holes of the central shaft, the deformation caused by water loss was smaller. FBG5 was laid at the bottom of the sand layer, and the deformation of the sand layer -was relatively small in the beginning. Yet when aquifer lost water only via the bottom of the drainage holes, the porosity rose and the deformation of aquifer increased linearly during the monitoring of sensor FBG5 with time going on.



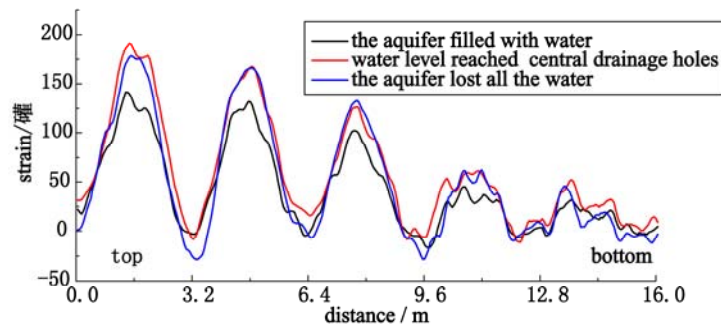
**Fig.7** Dependent variable of fine sand layer along with variation of time under water loss

Fig. 8 was the curve of circumferential strain of fine sand layer during its losing water, which was detected by BOTDA.

According to the change of water head value shown in fig 4, along with the curve of circumferential strain illustrated in fig 8, it can be found that affected by the loss of water in central drainage holes, with the reducing distance from the drainage holes, the porosity of the sand layer increased and the density decreased, so the circumferential deformation value of the fine sand layer increased, and the deformation value became stable while the change of water head decreasing.

According to the curves of circumferential strain in fig. 6 and fig. 8, we got circumferential strain distribution when the sand layer lost water without considering overburden pressure. At the same plane of sand layer, the circumferential deformation was connected with distance between the drainage holes, the variations of the water head value and the method of drainage.

When the drainage holes were set in the middle, because of water loss of the aquifer, the water head value changed obviously and the deformation increased, as the distance between water level and the drainage holes reduced. When the drainage holes were set at the bottom, affected by water quantity, only the water head value near the drainage holes changed and the circumferential deformation tended to change uniformly. In vertical direction, when water level of saturated fine sand layer decreased to the central drainage holes, the deformation near the drainage holes gradually decreased from top to bottom while the dependent variable far away from the drainage holes kept invariant without any variation in the water head value. When the pore water was excreted out of the aquifer only through the drainage holes at the bottom, the settlement of soil was homogeneous and the circumferential deformation was almost close to zero.



*Fig.8 Circumferential deformation of fine sand layer 40cm away from the shaft lining under water loss*

## Conclusions

(1) According to the monitoring results of settlement by FBG fiber Bragg grating technology, the vertical deformation of fine sand layer depends on water losing conditions and buried depth of the sensors. Under the same load, force on the soil at the bottom of shaft is smaller and the soil tends to be stable in a short time which deformation curve is significantly stepladder, while force on the soil on the top of shaft is larger and the soil tends to be stable for a long time. The hydraulic pressure drop of the soil on the top of shaft is larger and the deformation increases at the initial stage of water loss, while the deformation decreases gradually and tends to be stable with the hydraulic pressure drop reducing.

(2) The monitoring result of overburden layer based on BOTDA distributed optical fiber sensing technology shows that the circumferential deformation is related to the distance between the drainage holes, changes in the water head value and the method of drainage. When the drainage holes are set in the middle, with water level of saturated fine sand layer decreasing to the central drainage holes, the water head value, caused by the aquifer losing water, changes obviously as the distance between water level and the drainage holes reduces. Near the drainage holes, the deformation gradually decreases from top to bottom, yet when it is far away from the drainage holes, the dependent variable remains the same. When the drainage holes were set at both ends of the bottom, the pore water is running out only through the drainage holes at the bottom. Then it is only near the drainage holes that the water head value changes, and the circumferential deformation is almost in regular changes.

(3) Based on FBG fiber Bragg grating technology and BOTDA distributed fiber sensing technology, the study obtains deformation features of overburden layer under the water losing conditions, the result of which is consistent with the characteristics of overburden layer losing water simulated by MODFLOW software. It shows that, in monitoring shaft overburden layer, the placing technique and test method for optical fiber sensors are plausible.

## Acknowledgements

The work was funded by National Science Foundation for Youth (No. 51004103).

## References

- Cong LM (2006) Research on motoring and alarming system of shaft lining. Shandong University of Science and Technology 4
- Ding Y, Shi B, Cui HL, et al (2005) A fiber optic sensing net applied in slope monitoring based on Brillouin scattering. Chinese Journal of Geotechnical Engineering 27(3): 338-342
- Guo T, Li AQ, Song YS, et al (2009) Experimental study on strain and deformation monitoring of reinforced concrete structures using PPP-BOTDA. Sci China Ser E-Tech Sci 39(10): 1716-1724
- Hill KO, Fujii Y, Johnson DC, et al (1978) Potosensitivity in optical fiber waveguides: application to reflection filter fabrication. Appl. Phys. Lett. 32(10): 647-649
- Horiguchi T, Kurashima T, Tateda M (1989) Tensile strain dependence of Brillouin frequency shift in silica optical fibers. IEEE Photonics Technology Letters 1(5): 107-108
- Kishida K, Li CS, Lin S, et al (2004) Pulse pre-pump method to achieve cm-order spatial resolution in Brillouin distributed measuring technique. Technical report of IEICE, OFT 47: 15-20
- Lv HL, Yang WH, Cheng XL, et al (1997) The research on mechanism and control techniques of the shaft lining rupture under special strata(the second). Journal of China University of Mining & Technology 26(2): 1-4
- Liu ZQ, Zhou GQ, Zhao GS, et al (2005) The control method and its application about the soil grouting reinforcement process in vertical shaft. Journal of China Coal Society 30(4): 472-475
- Othonos A, Kalli K. Fiber Bragg gratings (1999) fundamentals and applications in telecommunications and sensing. London: Artech House
- Piao CD, Shi B, Wei GQ, et al (2008) Application of distributed fiber optic sensing techniques in bored pile detection. Chinese Journal of Geotechnical Engineering, 30(7): 976-981
- Sui WH, Zhang GL, Jiang ZQ, et al (2008) The state-of-the-art of chemical grouting treatment for quicksand hazards in coal mines and the prospect of several key problems. Journal of Engineering Geology 1 (Suppl.): 73-77
- Shi B, Xu XJ, Wang D, et al (2005) Study on botdr-based distributed optical fiber strain measurement for tunnel health diagnosis. Chinese Journal of Rock Mechanics and Engineering, 24(15): 2622-2628
- Zhu HH, Yin JH, Hong CY, et al (2010) Fiber optic based monitoring technologies of slope engineering. Geotechnical Investigation & Surveying (3): 6-9